Phase space approach for optimizing grid representations: The mapped Fourier method

Eyal Fattal, Roi Baer, and Ronnie Kosloff
Department of Physical Chemistry and the Fritz Haber Research Center, Hebrew University, Jerusalem 91904, Israel
(Received 11 August 1995)

The representation of a quantum system by an evenly spaced Fourier grid is examined. This grid faithfully represents wave functions whose projection is contained in a rectangular phase space. This is mathematically equivalent to a band limited function with finite support. In general, wave packets decay exponentially in classically forbidden regions of phase space. This idea is then used first to optimize the rectangular shape of the Fourier grid, leading to exponential convergence. Nevertheless, in most cases the representation is suboptimal. The representation efficiency can then be extremely enhanced by mapping the coordinates. The mapping procedure reshapes the wave function to fit into the rectangular Fourier shape such that the wasted phase space area is minimal. It is shown that canonical transformations, which rescale the coordinates, improve the representation dramatically. A specific scaling transformation enables the representation of the notoriously difficult Coulomb potentials. The scaling transformation enables one to extract almost as many converged eigenstate energies as there are grid points. The method is extendible to more than one dimension, which is demonstrated by the study of the H_2^+ problem. This scaling transformation can bridge the gap between quantum chemistry and quantum molecular dynamics by enabling the treatment of electronic problems in the vicinity of Coulomb potentials by grid methods developed for molecular dynamics.

PACS number(s): 02.70.Jn, 31.15.−p

I. INTRODUCTION

In a numerical approach to quantum mechanics the representation of the wave function is a key issue. Optimization of the representation is the focus of this study. A common approach is to use a spectral expansion in terms of a complete set of orthogonal basis functions. A truncated finite expansion is variationally the "best" with respect to this finite set of functions. Typically exponential convergence of the expansion can be obtained with respect to the number of expansion functions. This global approach to wave-function representation is best suited to the nonlocal character of quantum mechanics. An alternative representation is to express the wave function pointwise on a grid. This has to be supplemented by an interpolation scheme to express the value of the wave function between the grid points. The quality of the representation depends on the interpolation scheme. Low-order piecewise interpolation schemes converge quite slowly. With the use of global orthogonal interpolation functions a high-quality representation is obtainable with exponential convergence characteristics. This method is referred to as pseudospectral [1]. An important member of this family is the Fourier method, which uses the orthogonal collocation method as an interpolation scheme.

The design criteria for an optimal representation scheme are as follows. The scheme should be general so that it can easily be implemented to a series of related calculations. The number of representation functions or the number of grid points should be reduced drastically. This is because the numerical effort in quantum calculations scales as the cube of the number of points or functions for methods depending on diagonalization. For iterative methods depending on propagation the scaling is linear to squared in this number. These two design criteria can be in conflict. A general method is not optimized for a particular problem.

The Fourier grid method [2] based on a discrete Fourier expansion is an example of a very general method. A multidimensional representation is composed from a direct product of one-dimensional representations. The Fourier method has exponential convergence for almost any type of quantum wave packet. For a particular calculation one can obtain a more effective representation by choosing a specific set of expansion functions defined on a unique set of coordinate points. This fact makes each expansion function be local in coordinate space. In grid methods, this approach is known as the discrete variable representation (DVR) [3]. In multiple dimensions this can be supplemented by a sequential adiabatic reduction, thus leading to a highly specific and highly correlated expansion [4].

The purpose of this study is to find a method by which the representation efficiency of the Fourier method can be enhanced, thus creating a general and efficient representation scheme. The intuitive idea is simple. The Fourier method is based on a uniform sampling density of the wave function. Since for many quantum calculations the wave function is not uniformly distributed, a mapping procedure can enhance the sampling where it is needed. Mapping procedures have been suggested previously [2,5–10] and shown to be of practical use. But the analysis in these studies was heuristic, making it difficult to generalize. It is the purpose of this study to illuminate the physical reasoning leading to the enhanced sampling.

The most important realization in this study is that

the analysis of the mapping procedure has to be carried out in *phase space.* A nonuniform wave function is highly oscillatory in a restricted region of coordinate space. In a quantum mechanical language, there is a correlation between the position of the particle and its momentum. For example, a particle in a Morse potential has low momentum at the region of the outer turning point and high momentum at the region of the minimum potential value (region of high oscillations in the wave function). Moreover, the particle will have an exponential decreasing amplitude in regions of phase space that are classical forbidden. A phase space analysis based on the Wigner function [11] will reveal this observation. This means that a representation with exponential convergence has to cover uniformly the classical allowed region and have sufficient sampling ability in the classical forbidden regions.

The Fourier method represents a rectangular shape in phase space [2,12]. The optimized mapping procedure deforms this shape so that it matches the shape of the classical energy shell in phase space while maintaining the rectangular shape in the mapped phase space.

II. THEORY

A. Representation theory

A wave function $\psi(q)$ is represented on a grid by its values on the grid points $\psi(q_j) = \psi_j$. A continuous description of the wave function is obtained by interpolating between the grid points using an analytic set of basis functions $g_k(q)$:

$$\psi(q) \approx \bar{\psi}(q) = \sum_{k=0}^{N_g-1} a_k\, g_k(q)\ . \tag{2.1}$$

The expansion coefficients a_k are determined by matching the approximate solution to the true solution on the grid points,

$$\psi(q_j) \equiv \bar{\psi}(q_j) = \sum_{k=0}^{N_g-1} a_k\, g_k(q_j)\ , \tag{2.2}$$

which leads to a set of N_g linear equations for a_k if the number of grid points equals the number of expansion functions. The relation between grid points and expansion coefficients is called the collocation relation [2].

It is beneficial, both numerically and theoretically, to use a combination of grid points and orthogonal representation functions such that the functions are orthogonal when summed over the grid points:

$$\sum_{j=0}^{N_g-1} g_k(q_j) g_l(q_j) = \delta_{kl}\ . \tag{2.3}$$

This approach is known as the pseudospectral representation [1].

Specifically, in the Fourier method the grid points are equally spaced. The expansion functions $g_k(q)$ are the complex exponentials,which are both global and orthogonal:

$$g_k(q) = e^{i2\pi kq/L}, \quad k = -N_g/2, ..., 0, ..., N_g/2 - 1. \tag{2.4}$$

The N_g equally spaced sampling points are $q_j = (j-1)\Delta q$, $(j = 1, \ldots, N_g)$ where L is the length of the interval. The orthogonality of the basis functions $g_k(q)$ allows us to invert the collocation relation:

$$\begin{aligned} a_k &= \frac{1}{N_g} \sum_{j=1}^{N_g} \psi(q_j) e^{-i2\pi kq_j/L} \\ &= \frac{1}{N_g} \sum_{j=1}^{N_g} \psi(q_j) e^{-i2\pi kj/N_g}. \end{aligned} \tag{2.5}$$

The benefit of the Fourier method is that the the expansion coefficients a_k have a physical meaning, being interpreted as the discrete representation of the wave function in momentum space. The momentum space grid points are then $p_j = -p_{\max} + \frac{2p_{\max}}{N} j$. The Fourier method naturally reflects the symmetry between position and momentum spaces.

The basic criterion for constructing a converged representation in the Fourier method is understood from the the Whittaker-Kotel'nikov-Shannon sampling theorem [13–15]. The theorem states that band limited functions with finite support, sampled at equally spaced intervals can be interpolated with no loss of accuracy provided that $\Delta q < \frac{\pi}{K_{\max}}$. The function values in between the intervals are interpolated by a sum of sinc functions:

$$\psi(q) = \sum_{n=-(N_g/2-1)}^{N_g/2} \psi(n\Delta q)\ \text{sinc}\ [k_{max}(q - n\Delta q)]\,, \tag{2.6}$$

where the $\text{sinc}(x)$ function is defined as $\sin(x)/x$.

It is the dual relation of coordinate and momentum spaces seen in (2.5) that enables the analysis of the efficiency of the representation in terms of the classical or Wigner-Weyl phase space [11,16]. Since the sampling theorem refers to functions with finite range in both momentum and coordinate spaces, wave functions will be fully represented only if their phase space representation is fully confined within the (q,p) grid.

Wave functions in quantum mechanics belong to the class of functions L^2. Thus, examining the representation problem in quantum mechanics, wave functions in general are not strictly band limited functions and will not have in general finite support in coordinate space. Nevertheless, there is a class of wave functions that are exponentially close to band limited functions. This class of functions will be termed wave packets. For example, a Gaussian wave function is a wave packet since its amplitude outside a finite size interval can be made exponentially small in both coordinate and momentum pictures.

This leads to the physical origin of the wave packet: wave packets are a consequence of the fact that quantum mechanical wave functions decay exponentially in

the classically forbidden regions of phase space. Therefore a natural way of examining the representation properties of a wave packet is through its projection on phase space, and in particular by locating the classically allowed volume of phase space.

In the Fourier method the sampling points are equally spaced both in coordinate and momentum space. This means that the phase space representation of the grid has a rectangular shape. For a grid of 0 to L with N_g grid points $\Delta q = L/N_g$. The momentum range becomes $|p_{\max}| = \hbar\pi/\Delta q$, which leads to the relation between the phase space sampled volume $\mathcal{V}$ and the number of sampling points N_g [2]:

$$\mathcal{V} = 2\hbar\, \mathbf{L}\cdot\mathbf{k}_{\max} = N_g h\ . \tag{2.7}$$

This means that the grid can represent a maximum of N_g quantum states. The efficiency of the representation is defined as the ratio of the number N_e of converged eigenstates representable on the grid to the number of grid points:

$$\eta_c = \frac{N_e}{N_g}. \tag{2.8}$$

For representing a physical problem of energy E, the grid must enclose at least the classically accessible phase space volume Ω. Thus, a good estimate of the representation efficiency of a Fourier grid, which encloses the accessible phase space volume is the ratio

$$\eta_c \approx \frac{\Omega}{N_g h}. \tag{2.9}$$

As an example, the harmonic oscillator has an ellipse-shaped accessible volume in phase space. A simple canonical transformation transforms this ellipse to a circle in the new phase space. The optimal grid is then the smallest square, which encloses the circle, yielding the efficiency given by the area ratio $-\pi/4$. This result is an asymptotic result independent of the accuracy requirements [2]. It is a manifestation of the exponential decay of amplitude in the classical forbidden region and the exponential convergence of the Fourier representation.

These considerations can be used to construct an optimal grid for a Fourier representation. This is done by carrying out the following steps: (1) The energy range of the dynamical encounter is defined ($E_{\max}$). (2) The maximum energy value is used to find the confining classical boundary in phase space. For the coordinates $V(q_{\max}) < E_{\max}$, $V(q_{\min}) < E_{\max}$. And in momentum space: $P_{\max} < \sqrt{2mE_{\max}}$. (3) Once drawn, one looks for the smallest rectangle in phase space that contains the confining boundary. This rectangle then defines the Fourier grid, i.e., coordinates origin $q_{\min}$, length L, and spacing Δq, for each dimension. The sampling efficiency can be estimated by the ratio of the confined phase space "volume" to the volume of the rectangle since as stated above the wave-packet decays exponentially outside this boundary.

For a general problem, the classically allowed phase space shape can be quite irregular, resulting in a diminished sampling efficiency of the rectangular grid. Such a situation is depicted in Fig. 1.

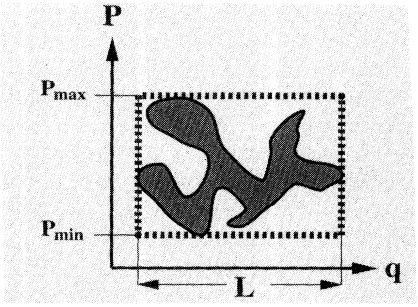

FIG. 1. Schematic representation of the confining boundary in phase space and the boundary of a Fourier grid. The optimal boundary of the Fourier grid is determined by the worst case scenario, leading to low sampling efficiency (ratio of the dark area to the rectangle area).

The phase space analysis initiated the exploration of the possibility of a canonical transformation, which deforms the rectangle grid shape in phase space, so that it will match the classical allowed volume boundaries. In the transformed coordinates, a rectangular grid will have an increased sampling efficiency.

B. Mapping procedure

The canonical transformation studied here is a mapping of the original set of N Cartesian coordinates $\{q_i\}$ to a new set of curvilinear coordinates $\{Q_i\}$, the scaled coordinates:

$$Q = Q(q,\alpha), \tag{2.10}$$

where α is a set of parameters. The mapping transforms the quantum problem to a new Hilbert space,

$$\Psi(Q) = \psi(q(Q)) \tag{2.11}$$

with a new scalar product,

$$\langle\Psi|\Phi\rangle = \int \Psi^*(Q)\Phi(Q)JdQ = \int \psi^*(q)\phi(q)dq \tag{2.12}$$

and a new kinetic energy operator:

$$\hat{\mathbf{T}} = -\frac{\hbar^2}{2m_j}\left[J^{-1}\frac{\partial}{\partial Q^j}\left(J\, g^{jk}\frac{\partial}{\partial Q^k}\right)\right];$$
$$J^2 = \det(g_{ij}), \tag{2.13}$$

where the convention of summation on repeated indices is used, J is the Jacobian of the transformation, g_{ij} is the Riemannian metric tensor,

$$g_{ij} = \frac{\partial q^k}{\partial Q^i}\frac{\partial q^k}{\partial Q^j}, \tag{2.14}$$

and g^{jk} is the matrix element of the inverse of (g_{ij}) matrix. As seen from Eq. (2.13), the mapping mixes the

coordinates (Q's) into the kinetic energy operator, thus inducing a correlation between the kinetic and potential energies of the problem. This observation can serve as an intuitive guide for choosing a transformation to suit a particular problem.

Once performed, the numerical implementation using the Fourier method is analogous to the Cartesian grid implementation. A equidistant grid is selected in the Q space. This is the new working grid. The wave function is represented by its values on grid points: $\Psi_j = \Psi(Q_j)$. Space-diagonal operators are implemented by simple pointwise multiplication and derivatives are implemented by transforming to the momentum P space, using the simple fast Fourier transform (FFT) procedure. In one dimension, for instance, the kinetic energy operator can be written as

$$\hat{\mathbf{T}} = -\frac{\hbar^2}{2m}\left(J^{-1}(Q)\frac{d}{dQ}\right)^2, \qquad (2.15)$$

where $J = \frac{dq}{dQ}$. Thus the kinetic energy operation can be implemented by a double evaluation of the first derivative multiplied by J^{-1}. The overall evaluation requires four Fourier transforms per operation compared to two Fourier transforms for the rectilinear implementation. If the mapping function is expressed in an analytically tractable form, the analytical form for the Jacobian derivatives can be used reducing the number of FFT's to three, instead of four.

The uniform sampling of the transformed coordinate (Q) results in a nonuniform sampling of the original coordinate q (see, for example, Fig. 2). Thus, an additional guide for constructing a good mapping is the location of the regions in q coordinate space, which need a dense grid-point representation.

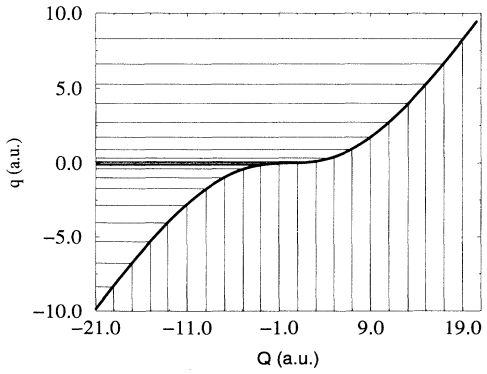

FIG. 2. The relation between grids of the Cartesian coordinate $q \equiv r$ and the mapped coordinate Q given by mapping function in Eq. (3.3) with the parameters $\beta = 0.1$ $A = 9.9$. Notice the congestion of sampling points near the origin (in the $[-10, 10]$ interval) of the q coordinate, as appropriate for Coulomb problems.

III. A MAPPING FUNCTION FOR THE COULOMB PROBLEM

A. Coulomb eigenfunction representation

The hydrogenlike Coulomb problem can be solved analytically. Yet, this potential is notoriously difficult to deal with using the regular Fourier method. It is therefore of great interest to extend the Fourier method to treating Coulomb potentials. This extension will enable the application of the Fourier method to solve density functional problems [17].

For a hydrogenlike system, the radial Schrödinger equation for the Coulombic potential is given by

$$\left[-\frac{1}{2m}\frac{\partial^2}{\partial r^2} - \frac{1}{r} + \frac{l(l+1)}{2mr^2}\right]\psi = E\,\psi, \qquad (3.1)$$

where $\psi = rR_{n,l}$ ($R_{n,l}$ are the so-called hydrogen radial functions). This equation is complemented by the $\psi(0) = 0$ boundary condition. The first problem one encounters in trying to solve this equation in the Fourier method is the boundary condition at $r = 0$. This is because the Fourier method insists on having a grid in which the wave functions and their derivatives go to zero in an exponential manner as grid length is enlarged. The common solution to this problem is to double the grid—over to the negative r side, and to consider only antisymmetrical wave packets since the symmetrical ones do not satisfy the $\psi(0) = 0$ boundary condition. This procedure does not increase the numerical effort since the number of operations can be reduced due to symmetry. The second problem is the singularity of the potential at the origin. The clearest way to observe the influence of the singularity is to examine the analytical behavior of the eigenfunctions. Consider the $1s$ radial eigenfunction, for example,

$$\psi_{1s}(r) = re^{-|r|}. \qquad (3.2)$$

Is this function a wave packet in the $(-\infty, \infty)$ $r = q$ space? Upon differentiating twice, one finds that the second derivative of this function at the origin is discontinuous, thereby leading to a non-wave-packet behavior: the function thus contains very high frequencies and one needs a very fine grid in order to represent it well. It should be noted that all the hydrogenic eigenfunctions have noncontinuous derivatives at $r = 0$.

The reason for the nonanalytical behavior of the $1s$ wave function is the singularity of the Coulomb potential both in q space and in p space. The q-space singularity is due to the infinity of potential at the origin. The p-space singularity is due to the long range of the potential and discontinuity of the derivatives of the wave function at the origin. Therefore, in order to correctly represent the hydrogenic radial wave functions using the Fourier method, one has to use both very dense and very long-ranged grids, leading to thousands of grid points even for the ground-state wave function.

In constructing a mapping to suit the Coulomb prob-

lem, one should notice that because these two demands result from two different singularities, they can be separated. The first demands dense grid points near the origin (singularity at the origin of q space). The second demands long-ranged grids (singularity at the origin of p space). This leads to the choice of a mapping function which maps uniformly sampled points in Q space to dense points near the origin in q space while leaving some sparse points in the long range of the potential.

B. A mapping function for the Coulomb problem

Considering the dual requirements the following mapping function has been found to be appropriate:

$$r = Q - A\arctan(\beta Q), \tag{3.3}$$

where r is the distance of the electron from the hydrogen nucleus and Q is the scaled coordinate. Since $\arctan(\beta Q)$ is a bounded function, for $Q \gg A$, $r \approx Q$. On the other hand, in an interval of $2\beta^{-1}$ around the Q origin, the arctan term causes a congestion of grid points in the r space around its origin. This can be seen in Fig. 2.

The phase space analysis allows us to examine the accomplishment of the mapping function in terms of representation efficiency as defined in Eqs. (2.8) and (2.9). First, the classical phase space shape is examined. Using a 32-point grid, spanning $[0, L]$, the maximum momentum becomes $p_{\max} = N\pi/L$. This creates a rectangle phase space of volume $\mathcal{V} = 2p_{\max}L = 2\pi N$. The energy of the hydrogen nth wave function is $E = -1/2n^2$. This energy determines the classically available phase space by the condition:

$$\frac{p^2}{2} - \frac{1}{q} > E. \tag{3.4}$$

In the scaled phase space the available volume is given by

$$\frac{P^2}{2J^2} - \frac{1}{Q - A\arctan(\beta Q)} > E, \tag{3.5}$$

where $J = 1 - \frac{\beta A}{1+(\beta Q)^2}$.

To demonstrate the scaling for $L = 800$ the following scaling parameters $A = 3999.9$ and $\beta = 0.00025$ are chosen (these parameters are chosen such that the mapped phase space energy shell is completely included within grid rectangle). Figures 3 and 4 show the series of classical energy shells of up to $n = 20$ for the unmapped and mapped grids, respectively. As can be seen, in the unscaled case a large portion of the classically available phase space is not represented by the grid.

This part corresponds to high momentum at small q. The missing phase space volume can be calculated. For example, the volume of the $n = 20$ energy shell is determined by the Born-Sommerfeld quantization rule [18] as $\mathcal{V} = 2\pi n = 125.7$. The volume contained in the grid is calculated as

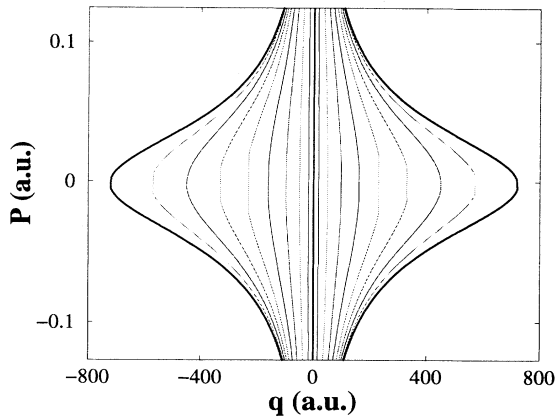

FIG. 3. The part of the energy shells $n = 1, 3, ..., 20$ which is represented by the grid rectangle in the unscaled phase space. It is seen that the grid cannot represent the high momentum part of the phase space. The shape of the phase space corresponds to a grid of 32×2 points with $L = 800$.

$$\mathcal{V}_{\text{inside}} = \int_{-p_{\max}}^{p_{\max}} q(p)dp, \tag{3.6}$$

where $q(p)$ is the energy shell of $n = 20$. In this case this integral comes out to be about 95, which means that 24% of the phase space of the problem is not represented within the defined Fourier grid. The scaling transformation squeezes into the grid the entire energy shell except for a very narrow corridor close to the origin at $Q = 0$, as seen in Fig. 4.

Here, the whole phase space of the problem is squeezed into the new phase space rectangle. Now, typical values of momentum are very low compared to those needed in the unmapped case leading to low sampling density

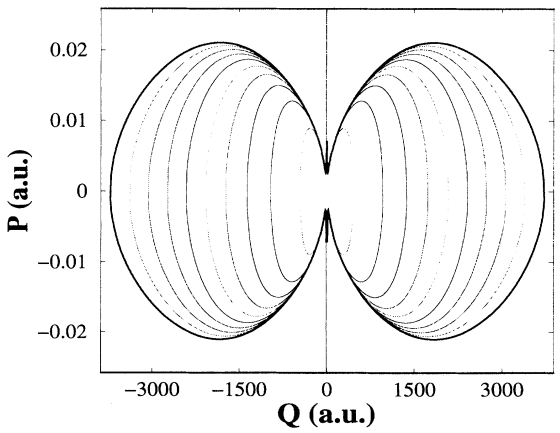

FIG. 4. The part of the energy shells $n = 1, 3, ..., 20$ which is represented by the grid rectangle in the scaled phase space. It is seen that the grid covers all the shells up to $n = 20$. The shape of the scaled phase space corresponds to grid of 32×2 points with $L = 3881$. The extremely narrow feature at $Q = 0$ should be noticed.

demand at the working grid.

Using this scaling the eigenstates of the hydrogen atom are calculated by direct diagonalization of the Fourier grid Hamiltonian. The difference between the calculated and theoretical energies are shown in Fig. 5.

It is seen that up to $n = 22$ the correct energy is reconstructed up to 3 digits at least, and that the accuracy declines sharply after that. Energies with $n > 22$ lose precision rapidly with increasing n. In many cases the accuracy is much better than 3 digits. The source of the inaccuracy is due to the quantum nature of the wave function, which leaks beyond the classically allowed energy shell. This can be demonstrated by looking at the Wigner distribution of the $1s$ state for the scaled and unscaled function as shown in Figs. 6 and 7.

Most of the amplitude of the Wigner distribution is within the classical energy shell. This means that the unscaled distribution extends outside the grid. This can be seen more clearly in the stereoscopic projection. The scaled distribution becomes localized in the grid, with a significant part of the amplitude within the classical energy shell. The small peaks on the $Q = 0$ line should be noticed. These peaks are localized on the Coulomb singularity.

A similar behavior is found for the $16s$ state (Fig. 8). Most of the amplitude is localized very close to the energy shell. Inside the energy shell a highly oscillating behavior is found and exponential decay outside. As in the $1s$ case, the $Q = 0$ line localizes some amplitude.

The sampling efficiency can be estimated by inspecting the outermost energy shell in Fig. 4. The ratio in area is approximately 62% and is consistent with the ratio of 20 converged eigenstates to 32 grid points, as predicted. Note also that the unscaled coordinates in the same grid are not able to reproduce any eigenenergy to a reasonable accuracy.

As mentioned above, one manifestation of the severe problem of Coulomb wave-function representation on a Fourier grid is the fact that there is a discontinuity in the higher derivative at $q = 0$. The mapping is able to reduce the effect of this singularity but is not able to eliminate it completely. This can be observed by studying the scaling of relative error with the size of the grid or the sampled phase space, Fig. 9.

For the ground state, initially the scaled grid converged much faster but eventually the asymptotic scaling for very large volumes of phase space is determined by the singularity at $Q = 0$. The asymptotic slope of ~ 2 is consistent with the discontinuity in the second derivative.

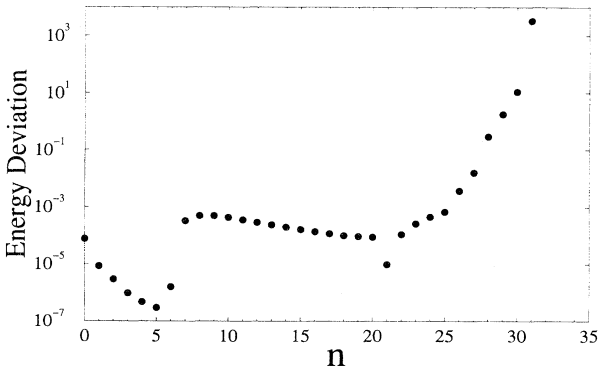

FIG. 5. Shown are the deviation between the calculated and the exact eigenenergies for the lowest 32 eigenstates calculated using scaled coordinates. A 64-point grid is employed in the range q $(-800,800)$ using the scaling parameters $A = 3999.9$ and $\beta = 0.000\,25$. The negative q side of the grid serves to impose the $\psi(0) = 0$ boundary condition, as discussed in the text. In accordance with the fact that the grid covers the $n = 20$ classical energy shells in phase space (see Fig. 4), energies with $n > 22$ lose precision rapidly with increasing n.

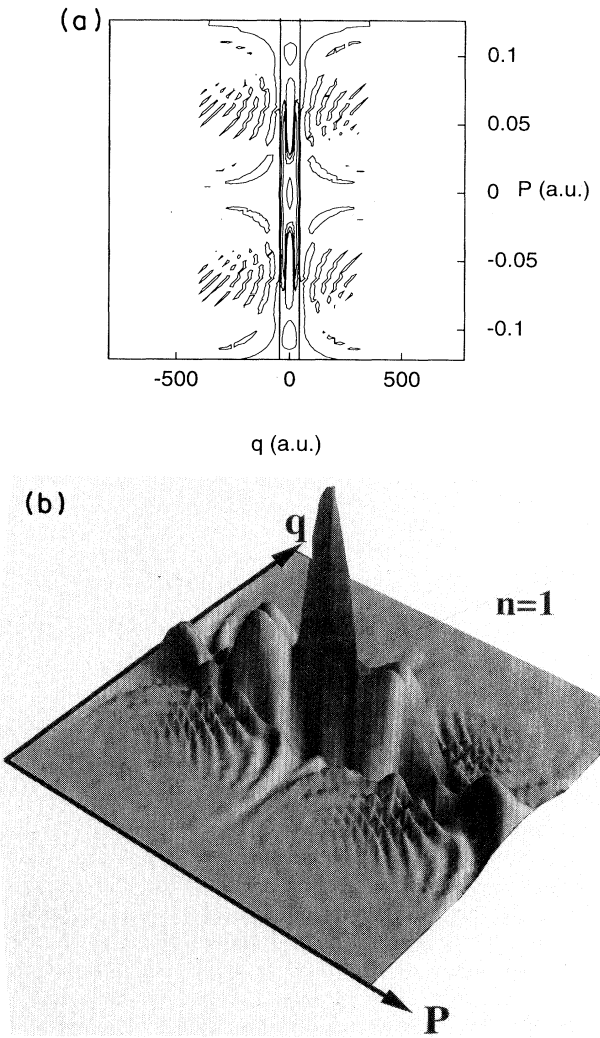

FIG. 6. The Wigner distribution representation on the Fourier grid rectangle of the $1s$ state in the unscaled coordinates. Calculated energy $E = -0.0378\,689$. (a) Contour plot. Superimposed is the classical phase space $1s$ energy shell shown as the two almost parallel lines around $q = 0$. (b) Stereoscopic projection.

When $l \neq 0$, the centrifugal barrier masks the Coulomb singularity in Eq. (3.1), making it easier to represent the wave functions. This can be seen by examining the scaling of the energy accuracy of the low-lying states in Figs. 9 and 10.

For the first excited state the uniform grid shows a scaling relation of ~ 3 consistent with the discontinuity in the third derivative at $q = 0$. The scaled grid shows an improved asymptotic scaling ratio of ~ 7.5.

It can be seen from Fig. 10 that the scaled functions converge faster for larger l values due to the softening of the singularity at the origin.

The Coulomb problem is an extremely difficult case. From the analysis it is clear that the mapping procedure has great advantages. In the next section the mapping is examined for a milder case.

C. Using the mapping for Morse potentials

The Morse oscillator serves as a generic system in molecular dynamics. At low energies the unharmonicities of the Morse oscillator vanish. This means that the sampling efficiency should be similar to the harmonic oscillator, i.e., $\pi/4$. For higher energies the phase space boundary becomes pear shaped and the sampling efficiency therefore decreases.

It has been shown that for a given number of grid points the sampling efficiency has a maximum for a specific grid spacing [2]. In order to compare the sampling efficiency for the uniform and mapped grids it is necessary to optimize the grid spacing for each case. For the mapped grid the mapping parameters were also optimized, where the same mapping function Eq. (3.3) was used.

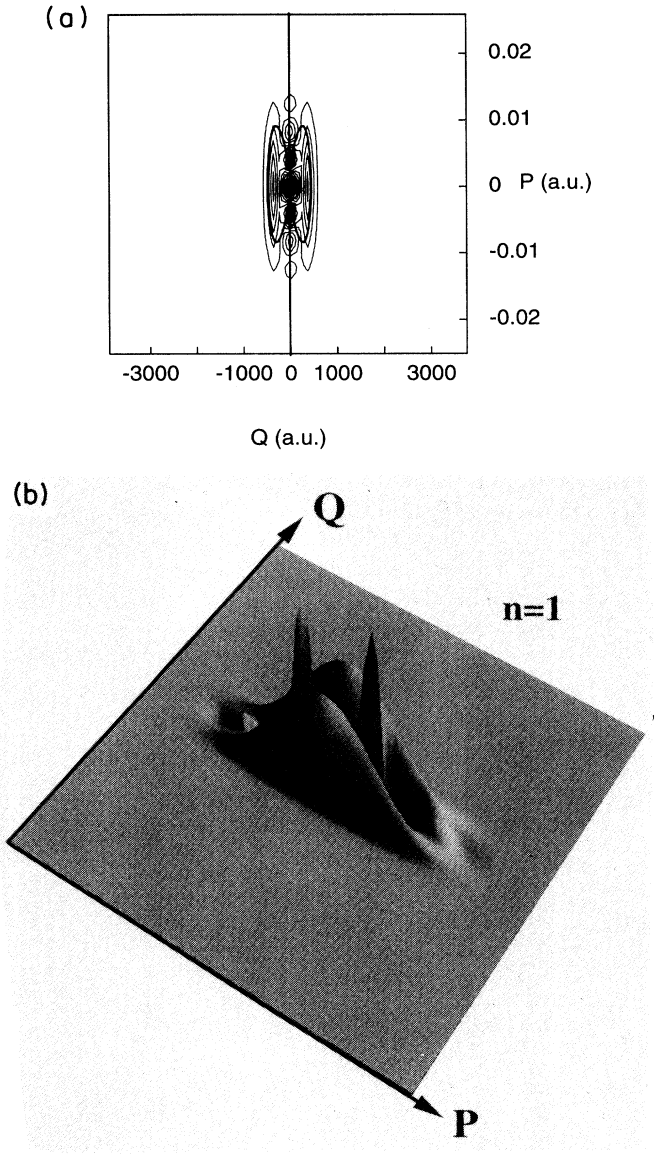

FIG. 7. The Wigner distribution representation on the Fourier grid rectangle of the $1s$ state in the scaled coordinates. Calculated energy $E = -0.499\,923$. (a) Contour plot. Superimposed is the classical phase space $1s$ energy shell. (b) Stereoscopic projection.

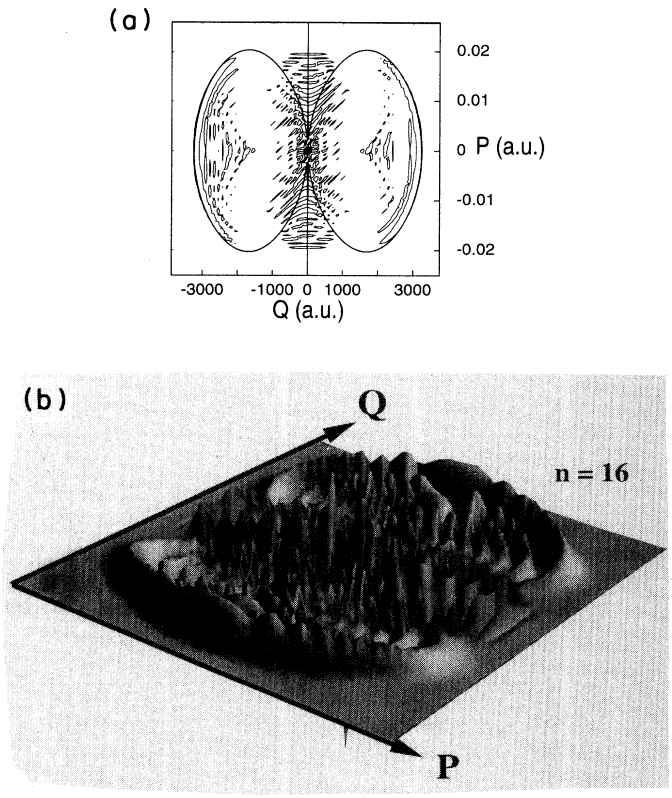

FIG. 8. The Wigner distribution representation on the Fourier grid rectangle of the $16s$ state in the scaled coordinates. Calculated energy $E = -0.001\,953\,04$ compared to $E_{\text{exact}} = -0.001\,953\,125$. (a) Contour plot. Superimposed is the classical phase space $16s$ energy shell. (b) Stereoscopic projection.

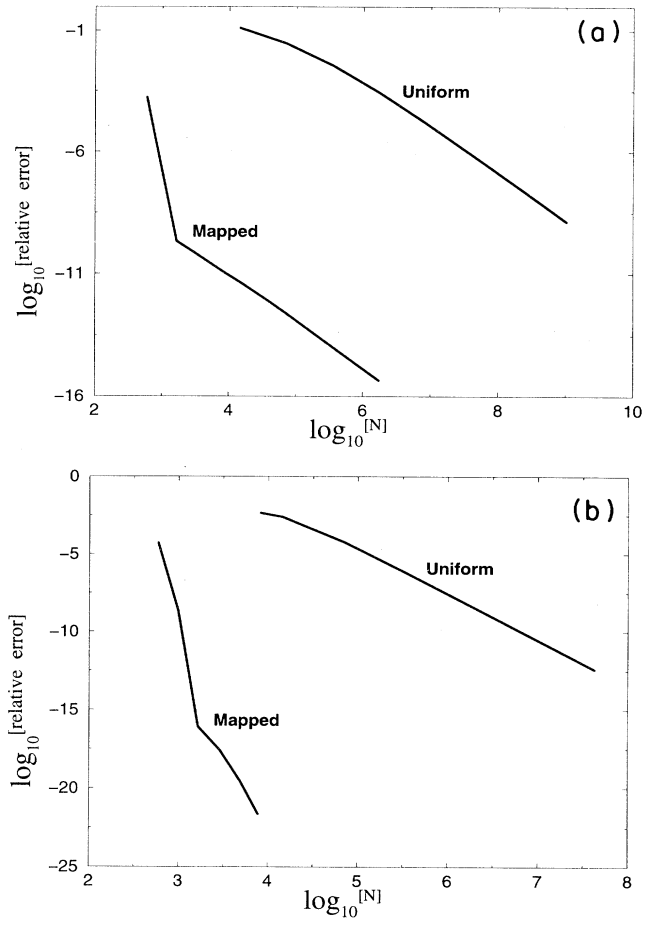

FIG. 9. The convergence of eigenenergy of hydrogen as a function of the number of grid points N_g. (a) $1s$ state, $\psi(r) = re^{-r/2}$. The asymptotic scaling law of the mapped grid has the same slope as the uniform grid. (b) $2p$ state, $\psi(r) = r^2 e^{-r/2}$.

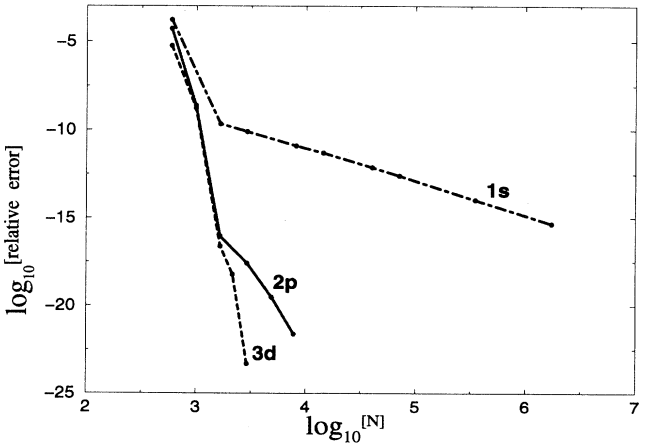

FIG. 10. The convergence of the energy of $1s$, $2p$, and $3d$ states as a function of the number of grid points N_g for scaled grids. This comparison shows the difference in behaviors due to the different character of the singularity of each case.

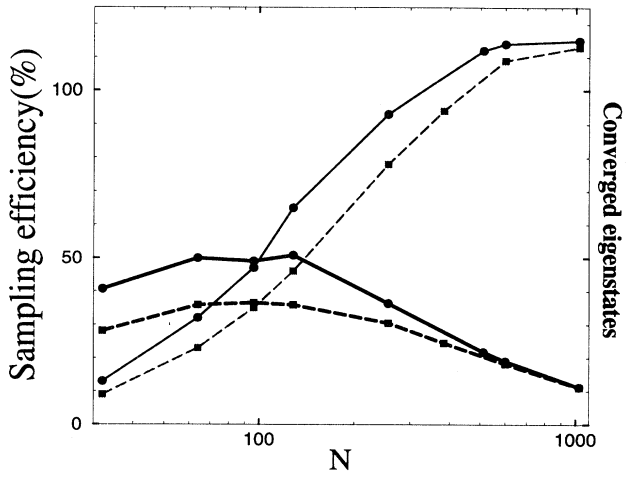

FIG. 11. Mapped and uniform grids sampling efficiency for the I_2 Morse potential (115 bound states). Sampling efficiency and the number of converged eigenstates (seven digits of accuracy in energy) vs $\log_{10}$ of number of grid points. Mapped (solid) and uniform (dashed). Each point on this graph is optimized with respect to grid spacing and mapping parameters.

The sampling efficiency of all the eigenstates of I_2 were examined (115 bound states). The results are shown in Fig. 11. The effect of improved sampling efficiency at a given number of sampling points in all mapped grids compared to uniform grids is clearly seen. Figure 11 refers to seven digits of precision in energy. The same behavior was found for higher precision calculations, which gave parallel results to those in Fig. 11.

For the Morse case better mapping functions can be found, i.e., a mapping function that exploits the fact that the potential is not symmetric with respect to the minimum.

IV. MAPPING IN TWO DIMENSIONS: THE DIHYDROGEN ION

The utility of mapping procedures increases with dimensionality since the reduction in the number of sampling points becomes crucial. This is the motivation for investigating a two-dimensional problem. The H_2^+ electronic wave functions were chosen for this study. Due to cylindrical symmetry, the system can be formulated as a two-dimensional problem with the Hamiltonian:

$$\hat{\mathbf{H}} = -\frac{1}{2\mu}\left[\frac{\partial^2}{\partial q_r^2} + \frac{\partial^2}{\partial q_z^2}\right] + \frac{m^2 - \frac{1}{4}}{2\mu q_r^2} + \mathbf{V}(q_r, q_z), \tag{4.1}$$

where q_r is the distance of the electron from the nuclear symmetry axis and q_z is the axial coordinate; the Coulomb attraction potential being

$\mathbf{V}(q_r, q_z) = -1/|\mathbf{q} - \vec{R}_1| - 1/|\vec{q} - \vec{R}_2|$ where $\vec{q} = (q_r, q_z)$ and $\vec{R}_i = (R_q^{(i)}, R_z^{(i)})$ is the coordinate of nucleus i. The boundary condition of the eigenstates is that $\psi(q_r = 0, q_z) = 0$. This forces an extension of the grid to negative values of q_r, and to antisymmetric wave functions with respect to the q_r coordinate, in a similar fashion to the hydrogen atom representation. For the angular momentum projection $m = 0$ in Eq. (4.1) the centrifugal term has an attractive part, which is singular at $q_r = 0$.

The mapping transformation of the Coulomb example Eq. (3.3) was used for each degree of freedom. The Riemannian metric tensor has the form

$$G = \begin{pmatrix} [Q_r - A_r \arctan(\beta_r Q_r)]^2 & 0 \\ 0 & [Q_z - A_z \arctan(\beta_z Q_z)]^2 \end{pmatrix}. \quad (4.2)$$

The conventions used are as follows: Q_r, Q_z are the mapped coordinates, and q_r, q_z are the unmapped coordinates.

The analytical (Born-Oppenheimer) results for this system were used for comparison. The energy for the ground state for a distance of 2 a.u. between the two nuclei was -1.10263 a.u. [19] (not including nucleus repulsion of 0.5). With a 16×16 mapped grid four digits of precision were obtained, while the unmapped grid was not able to converge even to one digit of precision. Similar results were obtained for excited states, for example, the lowest π level ($m = 1$), $E = -0.428\,711$ compared to the exact $E = -0.428\,775$, for a 16×16 mapped grid.

To observe and optimize the wave function in the four-dimensional phase space different cuts are required. Figure 12 shows the resulting ground-state wave function at the (Q_r, q_z) space. In optimizing the mapping parameters, only the mapping of the q_r coordinate was required. Mapping of the q_z coordinate hindered the convergence. The result of the mapping is a band limited wave function.

Figure 13 shows the ground-state wave function in the (P_r, P_z) space.

The classically available phase space for the ground state is determined by the condition

$$\frac{p_r^2}{2} + \frac{p_z^2}{2} - \frac{1}{|\vec{q} - \vec{R}_1|} - \frac{1}{|\vec{q} - \vec{R}_2|} - \frac{1}{4q_r^2} < E_{\mathrm{GS}}, \quad (4.3)$$

where $\vec{R}_i$ is the position vector of the nucleus. For this case the mapping is orthogonal and executed only on the q_r coordinate, therefore, $p_r = P_r/J$ (J is the Jacobian), $p_z = P_z$, $q_r = Q_r - A\arctan(\beta Q_r)$, and $q_z = Q_z$.

Figure 14 shows the (Q_r, P_r) cut through $q_z = 1$ of the classical phase space ground-state energy shell, of scaled and unscaled coordinates superimposed on the grid boundaries. It is clearly seen that the unscaled shell fails to fit into rectangular grid, while the mapped version fits well except for the very narrow corridor along $Q_r = 0$.

To examine the phase space structure of the wave function in the mapped directions the (Q_r, P_r) cut is informative. This cut is obtained by first taking the partial trace of the q_z coordinate to obtain the reduced density operator,

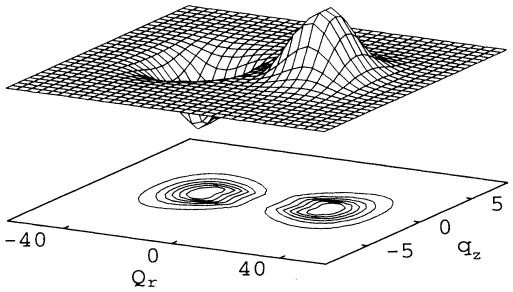

FIG. 12. The mapped H_2^+ ground state in (Q_r, q_z) space. Grid dimensions: q_r $(-10, 10)$, q_z $(-8, 8)$. All data are in atomic units. Q_r mapping parameters: $\beta_r = 0.02$ $A_r = 49.999$. Calculated energy $E = -1.102\,78$. The effect of mapping on the q_r coordinate can be seen. In the mapped (equally sampled) Q_r coordinate the wave function varies slowly. Also, from looking at the wave function at unmapped q_z coordinate it can be seen that it is slowly varying such that no scaling is indeed needed.

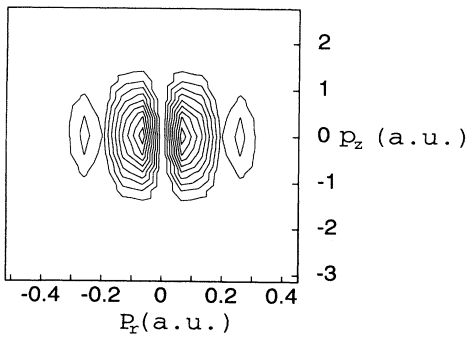

FIG. 13. The mapped H_2^+ ground state in (P_r, p_z) space (the P grid rectangle). The effect of mapping on the q_r coordinate can be seen. Values of the mapped P_r coordinate are very low, leading to low sampling density demand at the Q_r coordinate.

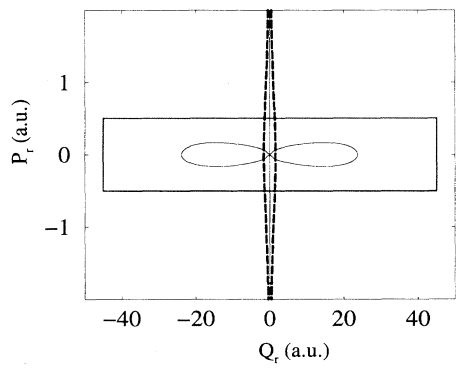

FIG. 14. The (Q_r, P_r) cut of the classical phase space ground-state energy shell, of scaled (solid) and unscaled coordinates (dashed). The cut is taken for the worst case in the mapped (Q_r, P_r) coordinates being $q_z = 1$ and $p_z = 0$. The rectangular box shows the boundaries of the Fourier grid. The effect of mapping is clearly seen as the scaled coordinates energy shell is contained within the Fourier grid phase space rectangle, while the unscaled coordinate energy shell spills out of the grid.

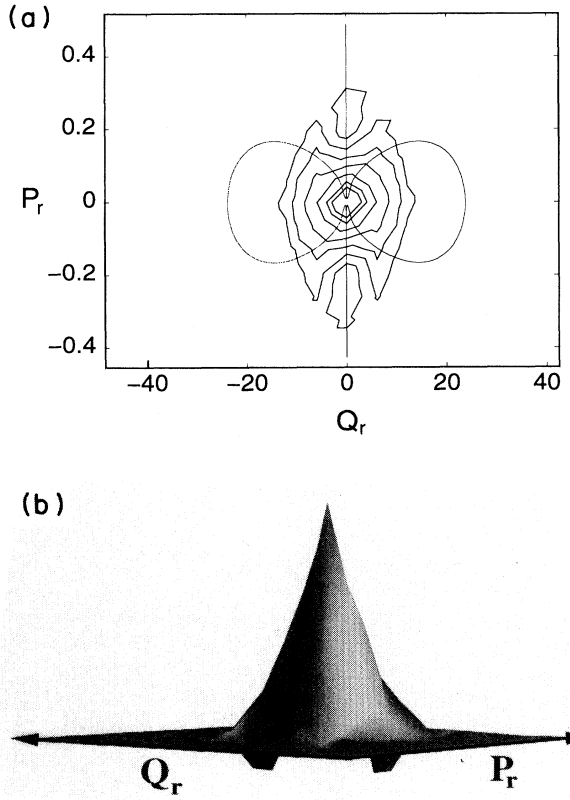

FIG. 15. The (Q_r, P_r) cut of phase space. The Wigner distribution representation on the Fourier grid rectangle of ground state. All data in atomic units. (a) Contour plot. Superimposed is the worst case classical ground-state energy shell. (b) Stereoscopic projection.

$$\rho(Q_r, Q_r') = \mathrm{tr}_{q_z}\left[\Psi(Q_r, q_z)\Psi^*(Q_r', q_z)\right]. \quad (4.4)$$

The Wigner distribution of the ground-state reduced density in the (Q_r, P_r) coordinates superimposed on the classical ground-state energy shell is shown in Fig. 15.

The ground-state Wigner distribution has a very distinct quantum character with negative amplitude on the $Q_r = 0$ singular line.

V. DISCUSSION

The ability to perform a quantum calculation depends crucially on the representation chosen. The computational effort scales with the number of representation points to some power. Moreover, excess representation points increase the spectral range of the Hamiltonian, which has a direct consequence on the convergence rate. For this reason methods that are able to reduce the number of representation points are extremely useful. It is also advantageous to pre-estimate the computational effort before the actual computation is carried through.

The phase space analysis developed in this study enables us to analyze the computational efficiency of the particular representation prior to its execution. If a low efficiency value is found reflecting a low ratio between the classical phase space volume contained in an energy shell and the phase space volume of the grid, then one is motivated to search for an enhanced sampling procedure.

The Fourier mapping procedure has great potential in enhancing the sampling efficiency. In the study of Refs. [7,8] a variational procedure was used to optimize the mapping function. The mapping function was represented as a Fourier series, which means that the Fourier coefficients were optimized. This procedure, which is based on the variational principle, is useful for the calculation of ground-state energy.

This study was motivated by dynamical calculations where a representation has to be optimized for a particular prespecified energy band containing the dynamical event. This fits the use of iterative propagation schemes where both time-dependent and time-independent information on the dynamical encounter can be obtained simultaneously [20]. For such calculations the phase space analysis based on the energy shell boundary is extremely useful [17].

The Fourier mapping procedure is a generalization of coordinate transformation technique. A common use is to reduce the number of degrees of freedom, thus improving efficiency. This approach was used on both the Coulombic and H_2^+ examples.

The detailed study of the Coulomb cases that have strong singularities was used to establish the phase space analysis tool. These singularities have hindered the use of the Fourier grid method in the past. The influence of these singularities on the convergence rate for the mapped and unmapped grids was found to follow the wave-packet criteria. The Coulomb case required an analytic mapping function. This is similar to the singular cases studied in Ref. [6]. The mapping function used was not unique; it appears that many useful mapping func-

tions will be found.

The mapped Fourier method is advantageous both as a general method and because of the ability to optimize it prior to execution. The phase space analysis was developed as the main tool used to optimize the sampling efficiency. This type of analysis should carry on to other problems and mapping procedures. As a result the sampling efficiency of the Fourier method will approach tailored basis set expansions with the advantage of the fast Fourier transform algorithm.

ACKNOWLEDGMENTS

We wish to thank Mr. Leonid Baranov for helpful suggestions. This research was supported by the Binational United States–Israel Science Foundation. The Fritz Haber Research Center is supported by the Minerva Gesellschaft für die Forschung, GmbH München, FRG.

[1] D. Gottlieb and S. A. Orszag, *Numerical Analysis of Spectral Methods: Theory and Applications* (SIAM, Philadelphia, 1977).
[2] R. Kosloff, in *Numerical Grid Methods and Their Application to Schrödinger's Equation*, edited by C. Cerjan (Kluwer Academic, Dordrecht, 1993), p. 175.
[3] J. C. Light, I. P. Hamilton, and J. V. Lill, J. Chem. Phys. **82**, 1400 (1985).
[4] R. A. Friesner, J. A. Bentley, M. Menou, and C. Leforestier, J. Chem. Phys. **99**, 324 (1993).
[5] B. Jackson, J. Phys. Chem. **93**, 7699 (1989).
[6] A. Bayliss and E. Turkel, J. Comput. Phys. **101**, 349 (1992).
[7] F. Gygi, Europhys. Lett. **19**, 617 (1992).
[8] F. Gygi, Phys. Rev. B **48**, 11 692 (1993).
[9] F. Gygi, Phys. Rev. B **51**, 11 190 (1995).
[10] F. Gygi and G. Galli, Phys. Rev. B **52**, R2229 (1995).
[11] E. P. Wigner, Phys. Rev. **40**, 749 (1932).
[12] R. Kosloff, in *Dynamics of Molecules and Chemical Reactions*, edited by J. Zang and R. E. Wyatt (Marcel Dekker, New York, 1995).
[13] E. T. Whittaker, Proc. R. Soc. Edinburgh **35**, 181 (1915).
[14] H. Nyquist, Trans. AIEE 1 **47**, 617 (1928).
[15] C. E. Shannon, Proc. IRE **37**, 10 (1949).
[16] M. Hillery, R. F. O'Connell, M. O. Scully, and E. P. Wigner, Phys. Rep. **106**, 121 (1984).
[17] Y. Zeiri, E. Fattal, and R. Kosloff, in Proceedings of the First Electronic Computational Chemistry Conference, Landover, MD, 1994, edited by S. M. Bachrach, D. B. Boyd, S. K. Gray, W. Hase, and H. S. Rzepa, ARInternet CD 101: paper 34.
[18] A. Sommerfeld, Ann. Phys. (Leipzig) **51**, 1 (1916).
[19] D. R. Bates, K. Ledsham, and A. L. Stewart, Philos. Trans. R. Soc. London **246**, 215 (1953).
[20] R. Kosloff, Annu. Rev. Phys. Chem. **45**, 145 (1994).

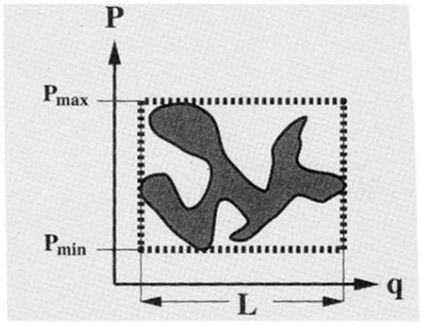

FIG. 1. Schematic representation of the confining boundary in phase space and the boundary of a Fourier grid. The optimal boundary of the Fourier grid is determined by the worst case scenario, leading to low sampling efficiency (ratio of the dark area to the rectangle area).

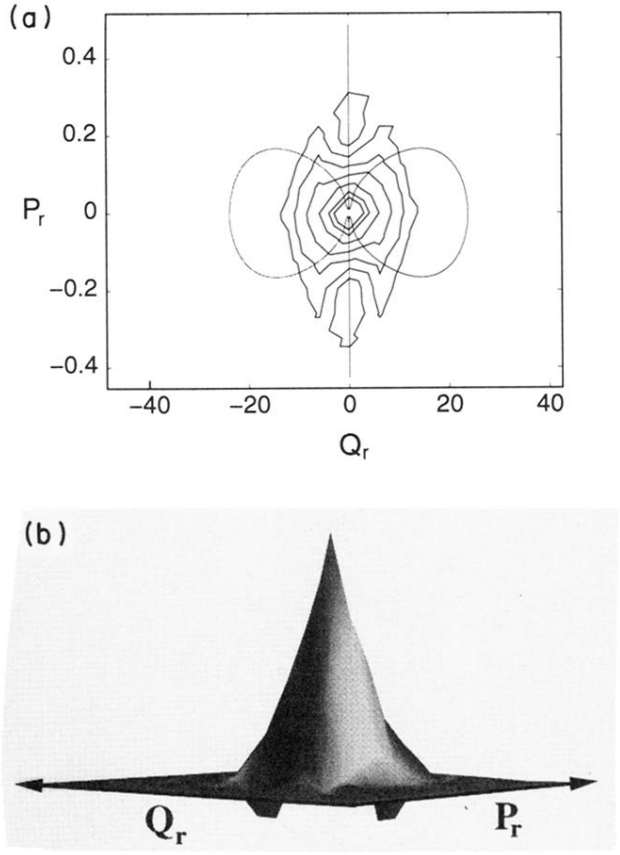

FIG. 15. The (Q_r, P_r) cut of phase space. The Wigner distribution representation on the Fourier grid rectangle of ground state. All data in atomic units. (a) Contour plot. Superimposed is the worst case classical ground-state energy shell. (b) Stereoscopic projection.

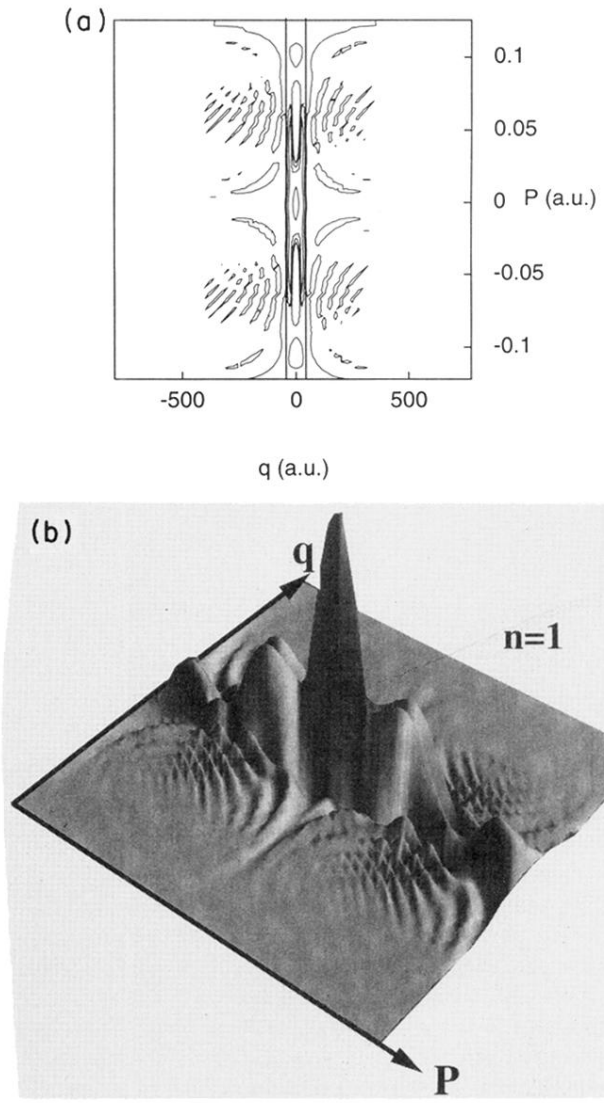

FIG. 6. The Wigner distribution representation on the Fourier grid rectangle of the $1s$ state in the unscaled coordinates. Calculated energy $E = -0.0378\,689$. (a) Contour plot. Superimposed is the classical phase space $1s$ energy shell shown as the two almost parallel lines around $q = 0$. (b) Stereoscopic projection.

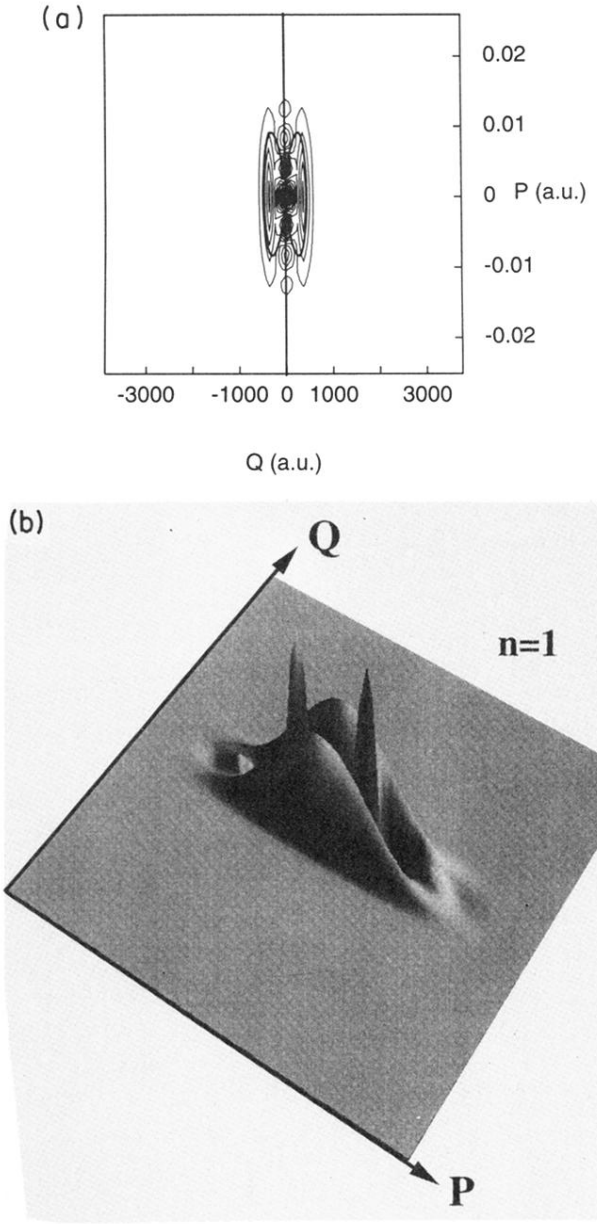

FIG. 7. The Wigner distribution representation on the Fourier grid rectangle of the $1s$ state in the scaled coordinates. Calculated energy $E = -0.499\,923$. (a) Contour plot. Superimposed is the classical phase space $1s$ energy shell. (b) Stereoscopic projection.

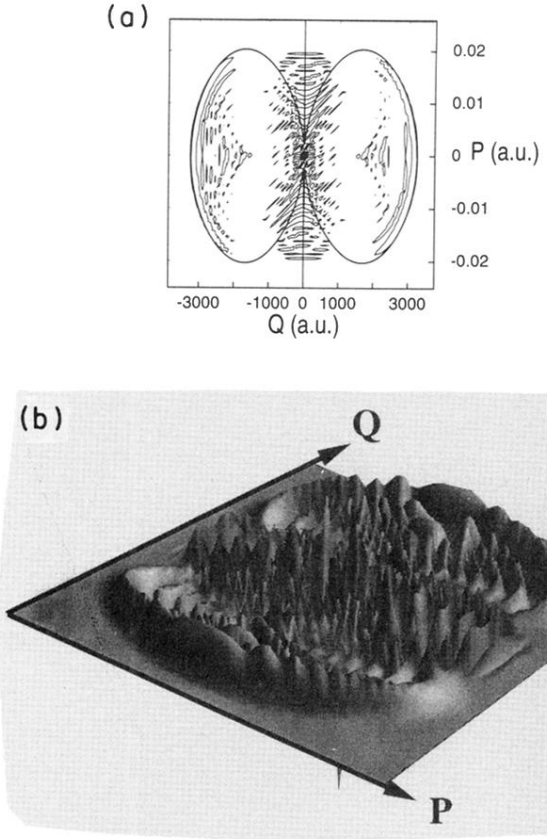

FIG. 8. The Wigner distribution representation on the Fourier grid rectangle of the $16s$ state in the scaled coordinates. Calculated energy $E = -0.001\,953\,04$ compared to $E_{\text{exact}} = -0.001\,953\,125$. (a) Contour plot. Superimposed is the classical phase space $16s$ energy shell. (b) Stereoscopic projection.